applied optics

Shock-related effects on aero-optical environment for hemisphere-on-cylinder turrets at transonic speeds

Jacob Morrida, Stanislav Gordeyev,* Nicholas De Lucca, and Eric J. Jumper

Department of Aerospace and Mechanical Engineering, University of Notre Dame, Indiana 46556, USA
**Corresponding author: Stanislav.V.Gordeyev.1@nd.edu*

Received 19 January 2017; revised 1 May 2017; accepted 6 May 2017; posted 8 May 2017 (Doc. ID 285093); published 31 May 2017

The aero-optical environment around a hemisphere-on-cylinder turret with both flat and conformal windows was studied experimentally in flight using the Airborne Aero-Optical Laboratory-Transonic for a range of subsonic and transonic Mach numbers between 0.5 and 0.8. Above $M = 0.6$, the local shock appeared near the top of the turret, causing additional aero-optical distortions at side-looking angles. Using time-resolved wavefronts, instantaneous shock locations were extracted and analyzed. The mean shock location was found to be near a viewing angle, $\alpha = 80$ deg for both window types at $M = 0.7$ and 0.8. For $M = 0.8$, the shock has a single frequency peak at $St_D = 0.15$, the same as for the unsteady separation line, indicating a lock-in mechanism between the shock and the separated wake region. Analysis of aero-optical distortions in the wake indicated that the wake dynamics were beginning to be affected by the shock only at high transonic speed of $M = 0.8$ for the conformal-window turret.

OCIS codes: (010.3310) Laser beam transmission; (010.7060) Turbulence; (010.7350) Wave-front sensing; (280.2490) Flow diagnostics; (280.7060) Turbulence.

https://doi.org/10.1364/AO.56.004814

1. INTRODUCTION

As it is desirable to have airborne directed energy and free-space communication systems that are usable at cruise speeds in the high transonic flow regime with hemisphere-on-cylinder turrets [1–4], a detailed study of the transonic effects on turrets and their aero-optical implications is needed. In the last decade, many experimental studies in tunnels [4–12], and numerous detailed numerical simulations [13–23] were carried out to understand the topology, dynamics, and aero-optical effects around turrets at fully subsonic speeds below $M = 0.5$.

Development of the Airborne Aero-Optical Laboratory (AAOL) program [1] provided a unique opportunity to collect aero-optical data around different turret geometries in realistic flight environments [24,25]. The impact of this program is hard to overestimate; for example, in 2013 a special issue of *Journal of Optical Engineering* with 19 papers [26] was devoted to analysis of aero-optical results collected with AAOL.

Recently, these aero-optical and fluidic studies were extended to transonic [15,16,27–35] and supersonic [16] flow regimes over various turret configurations. Flow over turrets is considered to enter the transonic flow regime for Mach numbers greater than 0.55 [4]. Above this critical Mach number, flow becomes locally supersonic on the turret and this supersonic flow region can affect the various flow features on the turret. Figure 1, top, shows the general flow features on a turret, and Fig. 1, bottom, shows additional effects in the transonic regime. The most notable difference from a turret in subsonic flow is the presence of a local unsteady shock on the turret. The shock strength intensifies with increasing Mach number. Due to the increased pressure gradients across the shock, it causes a premature wake separation above Mach number of ~0.7 [31]; they also result in additional optical distortions [30,34,36].

Spatial features of the shock were studied using planar laser-induced fluorescence (PLIF) at Mach 0.78 [32] and using oil-based surface flow visualization for a range of transonic Mach numbers [31]; limited studies of the shock-induced unsteady surface pressure field were conducted using pressure-sensitive paint (PSP) [35]. Recent conditional studies using planar image velocimetry (PIV) studies at Mach 0.8 [33] had shown the correlation between the shock position and the wake size. Important insight into the shock dynamics was obtained by studying unsteady shock around cylindrical turrets at transonic Mach numbers [36,37]; in particular, a lock-in mechanism was proposed to explain the observed correlation between the shock and the separation region [37]. All of these studies had confirmed that the wake dynamics is primarily affected by the shock, and not by the incoming boundary layer.

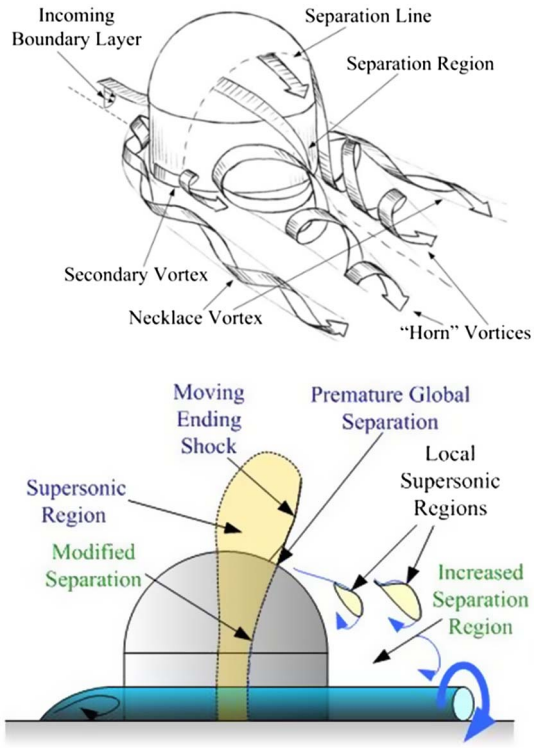

Fig. 1. Top: Flow topology around a turret at subsonic speeds. Bottom: Transonic flow features on the turret. Both images are from [4].

Because the shock is present only near the apex of the turret, the subsonic flow features around the turret are still present in the transonic regime. A necklace vortex forms as the boundary layer rolls up near the base of the turret and extends downstream. Whether shock induced or not, the separation occurs and forms a fully turbulent wake, with reattachment on the wall downstream of the turret. The upstream portion of the turret exhibits little turbulence, as the accelerating flow remains attached and the boundary layer is thin.

While tunnel tests with small turret models are very useful to study different physical aspects of the shock–wake interaction, to properly study the flow dynamics and related aero-optical effects for realistic turret-based systems, the Reynolds number, based on the turret diameter, should be larger than the critical Reynolds number of about 5,00,000 [4]. This means that the turret model should be large enough to satisfy this condition, requiring the usage of large tunnels. Furthermore, to eliminate blockage effects at high transonic speeds, one must use tunnels with porous tunnel walls. Finally, windows with good optical quality should be installed in a tunnel to collect aero-optical data at various field-of-regard angles. All these requirements significantly limit the number of available tunnels to perform aero-optical studies on turrets. To overcome these difficulties, a successful AAOL program [1] was extended into the Airborne Aero-Optical Laboratory-Transonic (AAOL-T) program [38], using faster Falcon 10 planes, capable of flying up to $M = 0.85$, to specifically study transonic aero-optical effects in flight.

Despite all the aforementioned studies, the details of how the shock affects the unsteady flow dynamics, including the unsteady pressure field and resulting unsteady forces acting on the turret, are not quite clear at this moment. Also, the exact effect of the unsteady shock on the aero-optical environment around turrets is still under investigation and is the main objective of this paper.

When a laser beam traverses through the turbulent region, the resulting aero-optical distortions are proportional to the integral of the density field in the propagation direction. Thus, wavefronts do not have any information along this direction and one should be careful interpreting the wavefront data. For instance, wavefronts cannot measure the extent of the shock into the flow or exact details of the shock lambda-structure near the wall. Nevertheless, spatially, temporally resolved wavefronts still provide useful information about the temporal variation and some spatial information about the turbulent flow.

This paper presents results of recent aero-optical flight measurements for the AAOL hemisphere-on-cylinder turret with different window geometries over a wide range of elevation and azimuthal angles for a range of Mach numbers between 0.5 and 0.8. Section 2 describes the experimental setup; the data reduction procedures are given in Section 3. Results are presented in Section 4, followed by conclusions in Section 5.

2. EXPERIMENTAL SETUP

Wavefront measurements were performed on the AAOL-T [38]. The AAOL-T program consists of two Falcon 10 aircraft flying in closed formation. The laser aircraft projects a diverging laser beam onto the aperture on the turret in the laboratory aircraft. Aircraft separation is maintained at approximately 50 m during the data collection. The turret, shown in Fig. 2, is a hemisphere-on-cylinder turret, with the diameter of $D = 1$ ft and the cylindrical height of 4 inches. The turret assembly has an optical window, which can be either flat or conformal, with aperture diameter of $A_D = 4$ inch. The turret assembly features a fast steering mirror (FSM) to stabilize the beam on the optical bench. Optical measurements were done the same way as during the AAOL program; for details of the optical setup, see [1,24,25], for instance.

Two separate flying campaigns were conducted to investigate aero-optics of the turret with different window geometries.

Fig. 2. Turret, with "smiles" covered, installed on AAOL-T.

During the first campaign, the optical environment around the flat-window turret was investigated at the following Mach numbers: 0.5, 0.6, 0.7, and 0.8. During this campaign, wavefront measurements were performed using a high-speed Shack–Hartmann wavefront sensor, based on a Phantom v711 camera. Like the data collection during the AAOL program, two different acquisition modes were used to measure wavefronts: slewing maneuvers and fixed-point data. Slewing maneuvers involved the laser aircraft moving relative to the laboratory aircraft while wavefronts were continuously acquired; these maneuvers allow for rapid mapping of the optical environment around the turret [24,25]. Fixed-point data involved the laser plane maintaining a fixed position with respect to the laboratory aircraft. These acquisitions were performed at a higher sampling rate, in order to investigate specific flow phenomena with a better temporal resolution. Wavefronts were collected with the spatial resolution of 32×32 subapertures and sample rates of 25 kHz for 0.7 s for fixed points and 3 kHz for 10–30 s for slewing maneuvers; durations were previously shown to be sufficiently long to have properly converged statistics [24]. Simultaneous with the 2D wavefronts, the overall beam jitter was also measured using a position sensing device. The jitter was acquired along with the turret azimuthal/elevation angle and FSM position information at 25 kHz for 10 s. Flight conditions were also recorded with the wavefront and jitter measurements. The aircraft separation was measured using a differential GPS system.

During the second campaign, the turret with both the flat and the conformal windows was flown at the Mach numbers of 0.5, 0.6, 0.7, and 0.8, and optical data at both fixed points and slewing maneuvers were collected. During this campaign, a faster Phantom v1610 camera was used, so wavefronts were collected with a better spatial resolution of 40×40 subapertures and sample rates of 30 kHz for 0.7 s for fixed points and 2 kHz for 15 s for slewing maneuvers. Simultaneous with the 2D wavefronts, the beam jitter was also measured using a position sensing device at 50 kHz for 30 s.

3. DATA ANALYSIS

Reducing the Shack–Hartmann images gives the measured wavefronts, W, as a function of location on the aperture and time. Through least-squares plane fitting, any residual instantaneous piston and tip/tilt were removed from the wavefronts, and the steady lensing was removed by removing the mean of the wavefront at every subaperture. The optical path difference (OPD) is the conjugate of the wavefront, $\mathrm{OPD}(\vec{x}, t) = -W(\vec{x}, t)$.

Both the beam direction and any point over the turret are characterized by the azimuthal (Az) and elevation (El) angles. From a fluid dynamics perspective, it is more useful to recast these angles into a different (α, β) coordinate system, illustrated in Fig. 3 [4,24]. A viewing angle, α, determines the angle between the incoming flow and the outward normal vector at any point on the turret, and the modified elevation angle, β, quantifies the angular distance from the wall of the aircraft. (α, β) angles are related to (El, Az) angles as

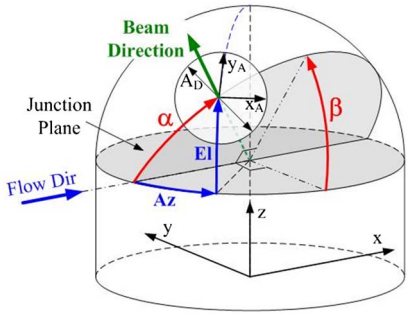

Fig. 3. Relationship between azimuthal (Az) and elevation (El) angles to viewing angle (α) and modified elevation angle (β) and the definition aperture-related frame of reference, (x_A, y_A). From [24].

$$\alpha = \cos^{-1}(\cos(\mathrm{Az})\cos(\mathrm{El})), \qquad \beta = \tan^{-1}\left(\frac{\tan(\mathrm{El})}{\sin(\mathrm{Az})}\right). \tag{1}$$

To compare the aero-optical performance of the turret across various Mach numbers, wavefronts were normalized by the flight conditions as

$$\mathrm{OPD}^{\mathrm{Norm}} = \mathrm{OPD}/\left(\frac{\rho}{\rho_{\mathrm{SL}}} M^2 D\right).$$

In this normalization, ρ is the freestream density, ρ_{SL} is the density at sea level ($\rho_{\mathrm{SL}} = 1.225\ \mathrm{kg/m^3}$), M is the Mach number, and D is the turret diameter. This so-called "ρM^2" scaling has been previously shown to collapse subsonic data acquired in flight and in the tunnel [4,24,25], and it is of interest to see whether this scaling still holds for transonic regimes.

A traditional way to represent aero-optical distortions over the aperture at different viewing angles is to determine a time-averaged *spatial variation* of the OPD across the aperture:

$$\mathrm{OPD}^{\mathrm{Norm}}_{\mathrm{RMS}}(\alpha, \beta) = \left(\overline{\langle \mathrm{OPD}^{\mathrm{Norm}}(x_A, y_A; t)^2 \rangle_{\text{over aperture}}}\right)^{1/2}. \tag{2}$$

Here (α, β) define the location of the aperture center, the angle brackets denote spatial averaging over the aperture points (x_A, y_A), defined in Fig. 3, the overbar defines temporal averaging, and t is time. $\mathrm{OPD}^{\mathrm{Norm}}_{\mathrm{RMS}}$ quantifies the amount of aberrations present in the beam for a specific viewing direction and can be used to estimate the far-field intensity on a target [39,40].

Another way to quantify the aero-optical distortions is to compute the *temporal variance* of the wavefronts at different points over the turret [25]:

$$S(\alpha, \beta) = \left(\overline{\mathrm{OPD}^{\mathrm{Norm}}(\alpha, \beta; t)^2}\right)^{1/2}. \tag{3}$$

Later in this paper, this quantity will be called the temporal variance of the wavefronts for brevity. It is important to distinguish between the quantities defined in Eqs. (2) and (3). $\mathrm{OPD}^{\mathrm{Norm}}_{\mathrm{RMS}}(\alpha, \beta)$ describes the *spatial* deviation of the aero-optical distortions over a *given aperture* and it is directly related to the far-field intensity [39,40]. This quantity depends on the aperture size, and angles α and β define *the location of the center of the aperture*. $S(\alpha, \beta)$ describes the *temporal* variation of aero-optical wavefronts at a given *point over the turret*, also characterized by α and β, and it is directly related to the strength of

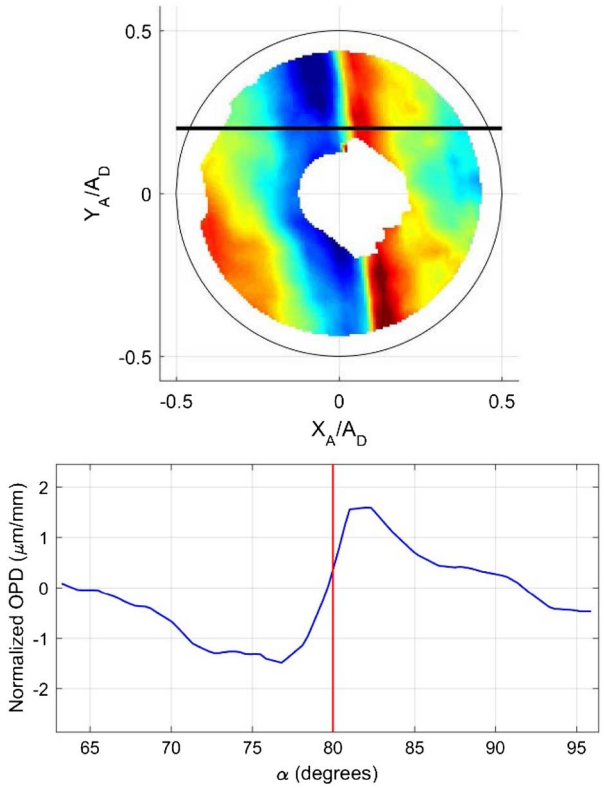

Fig. 4. 2D normalized OPD with black line representing 1D slice (top) and 1D slice of OPD with a red line corresponding to a shock location (bottom).

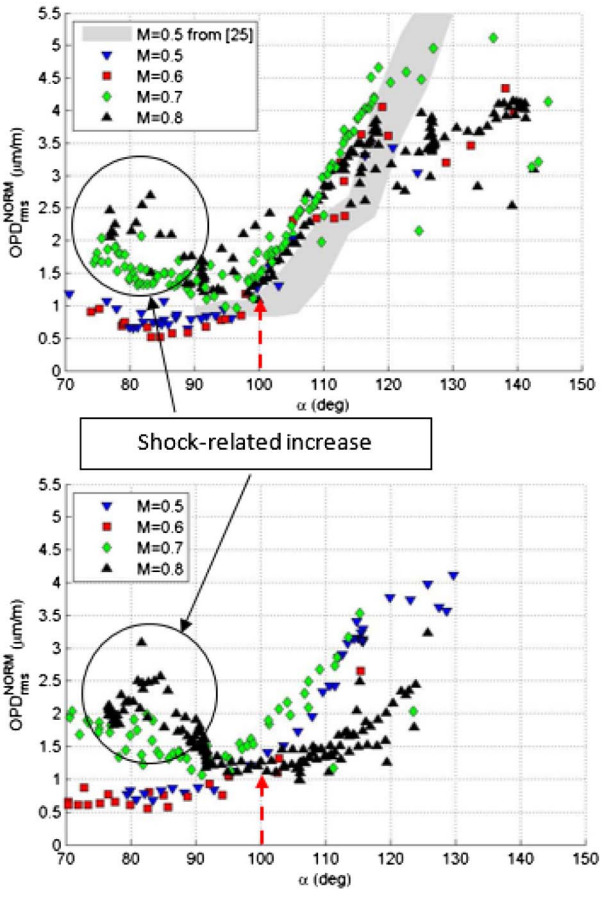

Fig. 5. Normalized OPD_{RMS} versus viewing angle for $M = 0.5$–0.8 for the conformal-window turret for a range of $\beta = 60$–90 deg (top) and $\beta = 20$–60 deg (bottom). Dashed red arrow indicates an approximate location of the flow separation. Comparison with results for the conformal-window turret with "smiles" from [25] is also presented.

aero-optical flow features; it is largely independent on the aperture size. Only fixed points were used to compute the converged temporal variance of the wavefronts, since in this case it is possible to relate the points on the aperture to the locations over the turret.

To quantify the temporal behavior of the wavefronts for a given viewing angle, the aperture-averaged, normalized wavefront spectra [41], were calculated:

$$S_W(f;\alpha,\beta) = \langle |\hat{W}^{\mathrm{Norm}}(f,\vec{x})|^2 \rangle_{\vec{x}\,\mathrm{over\,aperture}}, \quad (4)$$

where f is frequency, and S_W is the aperture-averaged, normalized wavefront spectra.

Since the shock causes a high-density gradient, which in turn causes high OPD variation, studying spatial–temporal variation of the wavefronts provides valuable insight in the dynamics of the shock motion. While the wavefront may not provide an exact shock location of the turret, simultaneous measurements of the wavefronts, shadowgraphs, and unsteady pressure of the surface revealed that there is a good correlation between the shock location and the sharp changes in the wavefront [29, 37]. Since in this paper only optical results are analyzed, any mention of the shock will mean the sharp increase in the wavefront, and the instantaneous shock location can be estimated by analyzing OPDs at each time step. An example of a wavefront is given in Fig. 5, top. As the optical system inside the turret has a small, one-inch diameter, middle obscuration, wavefronts are known only inside rings. To track the shock motion, a single β-angle, represented by a black line in Fig. 4, top, is chosen and the 1D OPD at that angle is extracted; see Fig. 4, bottom. The shock location was defined to be the location of the highest positive slope in the 1D OPD, shown as a red line in Fig. 4, bottom; a similar shock-tracking technique was used in [25].

4. RESULTS

A. Conformal-Window Turret

As the focus of this paper is the discussion of the additional aero-optical effects caused by the presence of the unsteady shock around the turret at high transonic speeds, relevant subsonic results will be described only briefly for the sake of completeness.

Temporal sequences of wavefronts at fixed points and during slewing maneuvers were analyzed, and normalized values of OPD_{RMS}, Eq. (2), were computed. Results as a function of the viewing angle, α, and Mach number for high-β angles, $\beta = 60 - 90$ deg, are presented in Fig. 5, top, and the results for low $\beta = 20 - 60$ deg are shown in Fig. 5, bottom. Convergence and uncertainty analysis, similar

to one in [24], (not presented here) gave the approximate relative error of aero-optical measurements as 5–10%. At subsonic speeds of $M = 0.5$, the flow is subsonic everywhere around the turret. As discussed in the Introduction, above the critical Mach number of 0.55, the local supersonic region with the resulting unsteady shock appears over the turret. However the shock is really weak and intermittent at $M = 0.6$ and does not affect the dynamics of the separated region [25]. The flow stays attached over the turret up to the viewing angle of approximately 100 deg with the low resulting $\mathrm{OPD_{RMS}}$, as the conformal window does not trip the flow around the window. Above $\alpha = 100$ deg, the flow separates and forms the unsteady separation wake downstream of the turret, resulting in progressively increased levels of the aero-optical distortions with the increasing viewing angle. Thus, the location of where $\mathrm{OPD_{RMS}}$ starts increasing can be used to estimate the location of the separation line. The "horn" vortices, formed on both sides of the turret close to the center plane, outlined in Fig. 1, top, caused additional distortions at high β-angles (see Fig. 5, top) compared with the distortions at the low β-angles (Fig. 5, bottom).

Results from previous flight tests at $M = 0.5$ of the same turret but with "smiles" uncovered at high α-angles are also shown as a shaded gray region in Fig. 5, top [25]. As the smiles were covered in the present tests and they were present in the tests reported in [25], comparison of aero-optical distortions with and without smiles, shown in Fig. 5, top, did not reveal any significant differences. It is an expected result, as the effect of the smiles on the vortical structures in the separated wake was shown to be confined primarily near the base of the turret [6], corresponding to low α-angles.

At higher transonic Mach numbers of 0.7 and 0.8, the unsteady shock intensifies and additional optical distortions related to the shock motion appear at the viewing angle of approximately 80 deg, seen as a local increase of the normalized $\mathrm{OPD_{RMS}}$ in Fig. 5. The flow is prematurely tripped by the shock at these speeds, causing an earlier separation over the turret [31]. Nevertheless, the normalized aero-optical distortions above $\alpha = 100$ deg for $\beta > 60$ deg (see Fig. 5, top) are approximately the same for both the subsonic and transonic Mach numbers, with slightly less values for $M = 0.8$, compared with the $M = 0.7$ case. For low β-angles, normalized optical distortions for $M = 0.8$ are also less than for the $M \leq 0.7$; see Fig. 5, bottom. Oil visualization of the surface flow topology around a hemisphere [31] had revealed that at high transonic speeds the increased interaction between the shock and the separated wake modified vortical structures in the wake. This increased interaction causes the horn vortices to move closer to the centerline, resulting in smaller distortions at low β-angles at high transonic Mach numbers, observed in Fig. 5, bottom. More on the wake response to the unsteady shock will be further discussed later in this paper.

Although not perfect, the approximate collapse of aero-optical data at high β-angles in the wake region for $\alpha =$ 100–120 deg indicates that the ρM^2 scaling, used to normalize aero-optical data, still can be used to re-scale data to different turrets and subsonic and transonic speeds. However, at side-looking angles the presence of the shock creates additional aero-optical effects and the scaling fails to collapse the data at these angles. A similar lack of collapse is evident for large $\alpha > 120$ deg, which in part might be attributed to sparse data at these angles.

Another way to study spatial features of the aero-optical distortions is to inspect the temporal variances of the wavefronts over the turret, defined in Eq. (3). As the conformal window does not change the turret shape, the temporal variance is independent of the aperture location and is related only to optical features of the separated wake. The temporal variances of wavefronts for different aperture positions were projected on the turret and were averaged in overlapping regions. The temporal variance of the wavefronts over the turret surface for $M = 0.6$ is presented in Fig. 6. Aero-optical distortions are small at the forward portion of the turret where the flow is attached. A region of increased distortion, related to the separation or wake region, which is dominated by horn vortices, is clearly visible. As the vortices are present on both sides of the turret, they create an additional velocity downwash in between them along the centerline; see Fig. 1, top. This increased downwash results in a smaller wake size along the center plane, with correspondingly smaller levels of aero-optical distortions for the increased range of α up to 125–130 deg. This region is labeled as a "quiet valley" in Fig. 6 and was also observed around flat-window turrets [24], and in numerical simulations of the flow around the conformal-window turret [13].

Similarly, temporal variances of the wavefronts were computed for transonic Mach numbers of $M = 0.7$ and 0.8 and the results are presented in Fig. 7. The shock creates additional localized distortions and they are clearly visible as a line of the increased distortions around $\alpha = 80$ deg. The shock-related optical intensity increases with Mach number, as expected. The average shock location is mostly independent of β. The quiet valley, while still present at these transonic speeds, is weakened and does not extend as far downstream, as for the $M = 0.6$ case. The horn-vortex-related region weakens as well and moves closer to the center plane at $M = 0.8$, compared to the $M = 0.7$ case; this indicates the changes in the separation wake dynamics due to the unsteady shock. The same trends were also observed around hemisphere-only turrets [30].

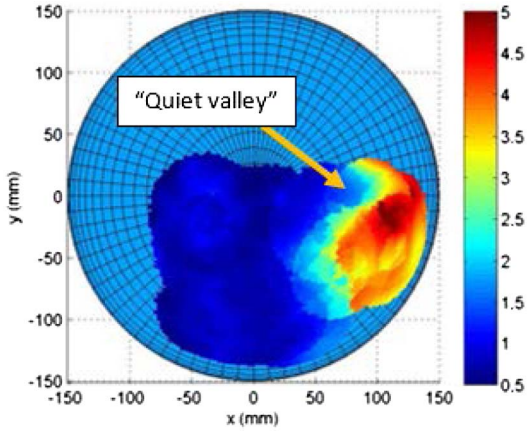

Fig. 6. Top view of temporal variance of the normalized wavefronts, $S(\alpha, \beta)$, (in μm/m) for the conformal-window turret at $M = 0.6$, with various flow features indicated. Flow goes from left to right.

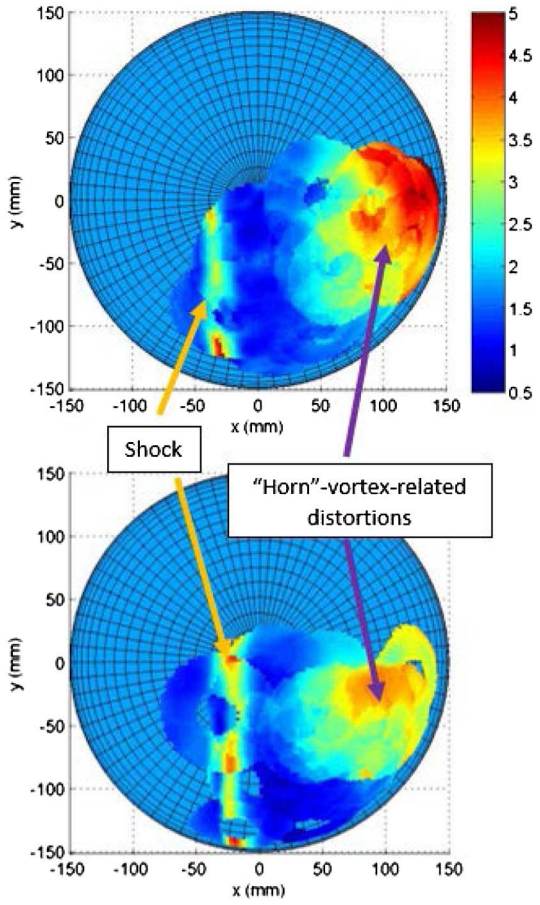

Fig. 7. Top view of temporal variance of normalized wavefronts, $S(\alpha,\beta)$, (in μm/m) for the conformal-window turret for $M = 0.7$ (top) and $M = 0.8$ (bottom), with the average shock location indicated. Flow goes from left to right.

A similar analysis of the aero-optical environment around hemisphere-only turrets has shown that the shock is located further downstream, around $\alpha = 85$ deg [30]. The exact reason that the shock appears more upstream for the full turret, compared to the hemispherical one, is not quite clear at this moment, and additional studies should be performed to see whether it is related to a particular flying platform or not.

A final comment about the maps of the temporal variance of the wavefronts, presented in Figs. 6 and 7, is that they provide useful non-intrusive means of studying spatial extent and intensity of density-varying structures in turbulent flows.

To study the temporal dynamics in the shock, spatial–temporal evolution of 1D slices of the wavefronts were extracted at different β-locations and Mach numbers, and the instantaneous shock location was extracted, as it was described before. Figure 8 shows a representative 1D slice of wavefronts taken at $M = 0.8$. The black dots represent the shock location for each time step; the shock motion is not periodic, but clearly has a single preferred frequency.

Using the instantaneous shock location, various shock-related statistics were computed and analyzed. Figure 9 depicts the time shock locations at different β-angles with bars representing the range of α where the shock is present 90% of the

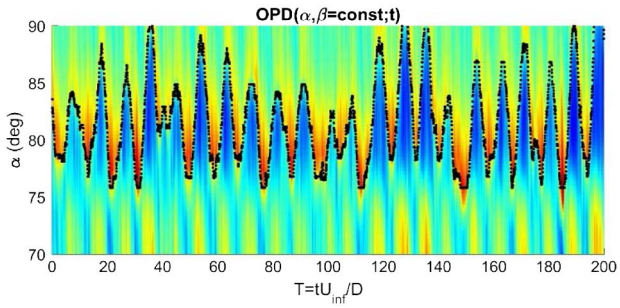

Fig. 8. Spatial–temporal evolution of 1D slice of OPD for $M = 0.8$. Black dots indicate the approximate shock location.

time. As it was already observed in Fig. 7, the mean shock location angle does not change significantly with changing β. For $M = 0.7$, the mean shock location tends to be at slightly lower angles than the mean angular values for a given β for $M = 0.8$.

The normalized spectra of the shock position for a conformal window at $M = 0.7$ and $M = 0.8$ are shown in Fig. 10. The main difference between the two is that the $M = 0.7$ case has two peaks around $St_D = 0.18$ and $St_D = 0.4$, while the $M = 0.8$ case has only one peak near $St_D = 0.15$. Pressure measurements in the turret wake have showed similar peaks for both $M = 0.7$ and 0.8 [42]. To understand a possible mechanism of this low-frequency dynamics, let us recall that a weaker, intermittent shock was observed over the conformal-window turret in flight at lower $M = 0.65$ with a typical frequency of $St_D \sim 0.5$ [25]. Also, $St_D = 0.15$ has been associated with the unsteady separation line motion over a wide range of subsonic [6] and transonic [42] Mach numbers. At low transonic speeds the shock is weak and mostly independent of the separation region dynamics. At higher Mach numbers the shock becomes strong enough to force a premature separation, effectively coupling or locking in the shock and the separation line dynamics. In Ref. [37] a strong coupling between the shock location and strength with the location and size of the separated region was studied over cylindrical turrets and an acoustical feedback was proposed as a plausible mechanism for locking the dynamics of the shock and the shock-induced separation region. Recent PIV studies of the flow around the hemisphere at Mach 0.8 [33] also suggest that a similar lock-in mechanism is present over the 3D turret.

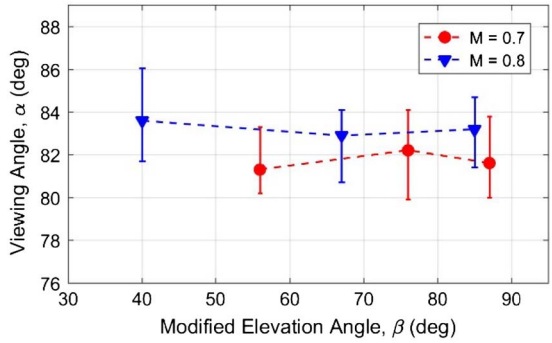

Fig. 9. Shock mean locations and 90% range for $M = 0.7$ and 0.8 for the conformal-window turret.

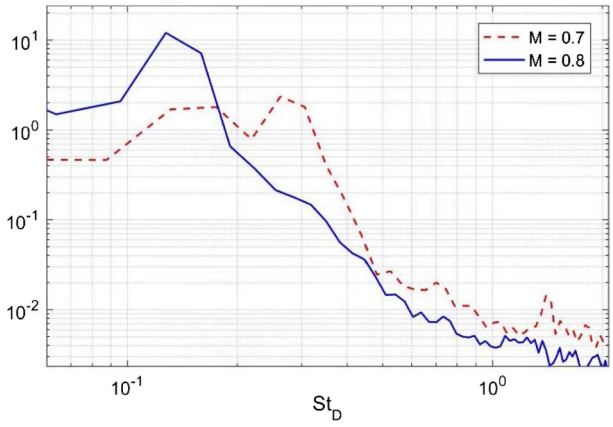

Fig. 10. Conformal-window normalized shock location spectra for $M = 0.7$ and 0.8. $\beta = 60$ deg.

To further study the temporal dynamics of the shock and the wake, the aperture-averaged wavefront spectra, defined in Eq. (4), were computed for all tested Mach numbers. Figure 11 presents the wavefront spectra at $\alpha = 80$ deg, where the shock is present at high transonic speeds. While spectra at low speeds of 0.5 and 0.6 are fairly weak, with one peak around the unsteady-separation-related value of $St_D = 0.15$, the spectrum for $M = 0.7$ shows two peaks around 0.15 and 0.3. At higher $M = 0.8$, the peak around 0.15 becomes dominant. At these Mach numbers, the optical distortions are primarily shock driven, so these peaks correspond to the peaks observed in the shock-motion spectra in Fig. 10.

Figure 12 shows the normalized wavefront spectra in the wake region for $\alpha = 120$ deg (Fig. 12, top) and for $\alpha = 140$ deg (Fig. 12, bottom). At $\alpha = 120$ deg, the spectra exhibit self-similar behavior for subsonic and transonic speeds with a peak at a higher frequency of around $St_D = 1.3$. This value is associated with smaller shear-layer structures forming in the wake [42]. Thus, while the shock causes the premature flow separation near the apex of the turret at high transonic speeds, after the flow is separated, the presence of the shock does not affect the dynamics of the shear-layer structures in the separation region, except for the highest Mach number of 0.8, where

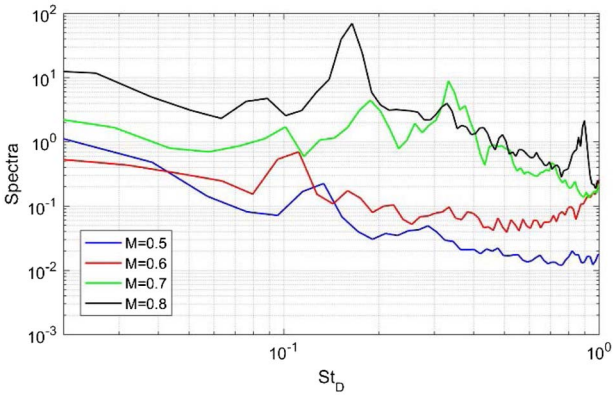

Fig. 11. Aperture-averaged wavefront spectra, $S(f)$, for the conformal-window turret for $\alpha = 80$ deg at different Mach numbers.

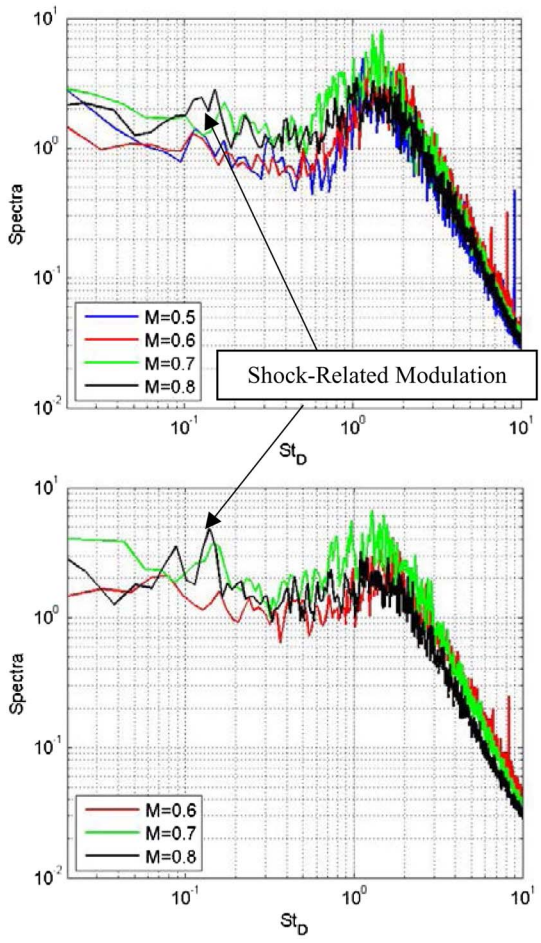

Fig. 12. Aperture-averaged wavefront spectra, $S(f)$, for the conformal-window turret for $\alpha = 120$ deg (top) and for $\alpha = 140$ deg (bottom) at different Mach numbers.

an additional small peak appears in the spectra at $St_D = 0.15$. Thus, the shock motion, associated with the lower frequency of $St_D = 0.15$, starts modulating or affecting the temporal evolution of the shear-layer structures in the wake at high transonic speeds. The modulation effect can also be observed at $\alpha = 140$ deg (see Fig. 12, bottom) where the peak at $St_D = 0.15$ is the same order of magnitude, as the shear-layer-related peak of $St_D = 1.3$ for $M = 0.7$ and $M = 0.8$.

B. Flat-Window Turret

The effect of the flat window on the flow and related aero-optical distortions around turrets at subsonic speeds was discussed in [24]. The main effect, related to the flat window, was observed at side-looking angles around $\alpha = 100$ deg, where a small separation bubble forms over the window, causing additional aero-optical aberration over a range of viewing angles between 90 and 100 deg. Figure 13 shows the normalized OPD_{RMS} values for the flat-window turret as a function of Mach number and the viewing angle. As the $M = 0.5$-case was extensively studied in [24], only few points for $M = 0.5$ were collected during this work, mainly for comparison and repeatability purposes. OPD_{RMS} values measured during these tests are very similar to values from [24], shown in Fig. 13 as a

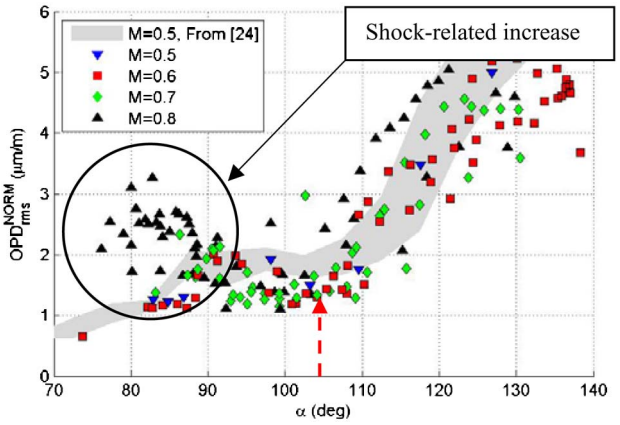

Fig. 13. Normalized OPD_{RMS} versus viewing angle for $M = 0.5$–0.8 for the flat-window turret for a range of $\beta = 50$–90 deg at different Mach numbers. Dashed red arrow indicates an approximate location of the flow separation. Comparison with results for the flat-window turret with "smiles" from [24] is also presented as a gray shaded region.

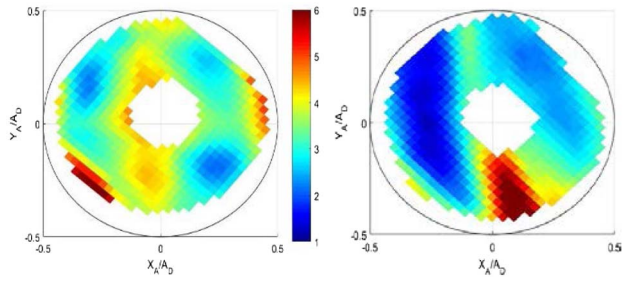

Fig. 14. Temporal variance of the normalized wavefronts, $S(\alpha, \beta)$, (in μm/m) over the flat-window aperture. Left: Az = 82 deg and El = 36 deg ($\alpha = 84$ deg), $M = 0.7$. Right: Az = 72 deg and El = 56 deg ($\alpha = 80$ deg), $M = 0.8$. Flow goes from left to right.

gray-shaded region. For both $M = 0.5$ and 0.6, OPD_{RMS} values are small for $\alpha < 90$ deg, as the flow is attached over the flat-window aperture. At $M = 0.6$ the local shock on top of the turret is too weak to modify the otherwise subsonic flow over the turret, so a similar separation-bubble-related peak in OPD_{RMS} around $\alpha = 90$ deg is present at $M = 0.6$; the peak location is slightly shifted forward $\alpha = 90$ deg, compared to the $M = 0.5$-case. At $\alpha = 110$ deg the flow separates, and for large viewing angles $\alpha > 110$ deg OPD_{RMS} continuously increases due to looking through the separated wake of the turret. Again, this behavior is very similar to OPD_{RMS} results at $M = 0.5$.

For a higher $M = 0.7$, the location of the local peak due to the separation bubble over the flat window is around 90 deg and approximately unchanged from $M = 0.6$. The local peak is sharper, compared to the $M = 0.6$ case; inspection of wavefronts has revealed the presence of the shock approximately in the middle of the aperture. The flow separates around 110 deg as well, and the normalized aero-optical distortions in the wake appear to be unchanged.

For $M = 0.8$, a stronger shock was found to be present over the flat aperture between viewing angles 75 and 90 deg, so the overall levels of OPD_{RMS} are significantly higher, compared to values at the same angle range at lower Mach numbers. The separation is also affected by the shock presence and appears to occur slightly upstream, at $\alpha = 105$ deg, compared to $M = 0.6$ and $M = 0.7$.

The normalized temporal variances of wavefronts are shown in Fig. 14 for two different Mach numbers. Both the $M = 0.7$ (Fig. 14, top) and $M = 0.8$ (Fig. 14, bottom) show an increase in OPD_{RMS} in a narrow band near the center of the aperture due to the presence of the unsteady shock. This is the mean shock location for both cases. Because the shock location is near the center of the aperture, even though the viewing angle and Mach number are slightly different between the two cases, it appears that the flat window has an "anchoring" effect on the shock and forces the shock to be near the center of the aperture. One possible reason for this anchoring effect is that the separation bubble forms a fluidic curved surface over the aperture. The topology of the separation bubble is very sensitive to the flat-window position, as well as the flow environment. For $M = 0.7$, the shock is formed over the curved fluidic surface, but the shock is too weak to modify it. The shock becomes stronger at $M = 0.8$, significantly modifying or even potentially destroying the bubble. Compared with the results for the conformal-window turret, presented in Fig. 5, the resulting OPD_{RMS} for both the flat and conformal windows is very similar at $M = 0.8$, confirming that at high transonic speeds the aperture geometry becomes a secondary factor, compared to the shock-induced effects. Also, similar to the conclusions with the conformal-window turret, presented earlier, the ρM^2 scaling, used to normalize aero-optical data, is still useful to re-scale data at high α-angles above 100 deg to different turret sizes and subsonic and transonic speeds.

Similar to the conformal-window case, the instantaneous shock location was extracted in α-direction for given fixed β. It was found that for both $M = 0.7$ and 0.8 the shock was present between $\alpha = 71$ and 87 deg 90% of the time, with the average location at 80 deg.

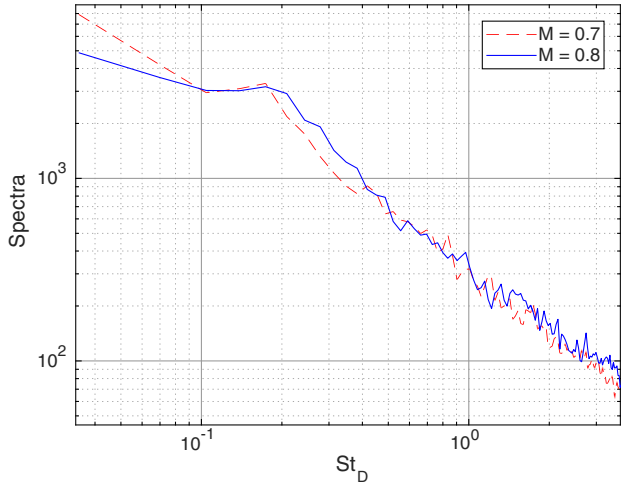

Fig. 15. Flat-window shock location spectra for $M = 0.7$ and 0.8, at $\alpha = 84$ deg, $\beta = 43$ deg.

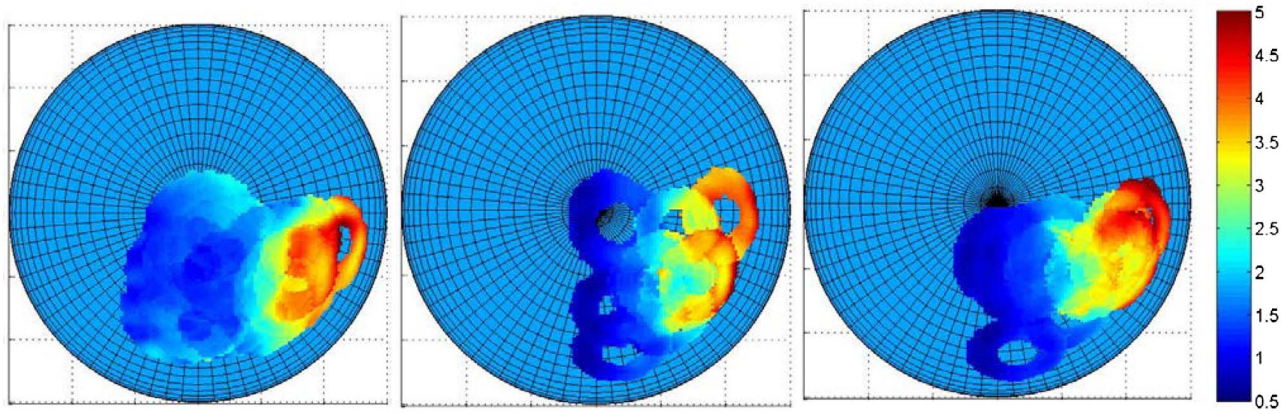

Fig. 16. Top view of temporal variance of normalized wavefronts, $S(\alpha, \beta)$, (in μm/m) for the flat-window turret for $M = 0.6$ (left), $M = 0.7$ (middle), and $M = 0.8$ (right). Flow goes from left to right.

The temporal spectra of the shock position for both $M = 0.7$ and $M = 0.8$ are shown in Fig. 15. There is not much discernable difference between the frequency content of the shock movement for the two Mach numbers. Both exhibit a single peak near $St_D = 0.15$, unlike for the conformal-window turret, where two peaks at 0.15 and 0.3 were observed for the $M = 0.7$ case. As stated before, this peak has been associated with the movement of the separation line on the turret. As the local separation bubble is sensitive to the global environment, which is primarily governed by the separated region downstream of the turret, this single peak in the shock spectra indicates that the shock dynamics is linked to the dynamics of the separation line.

To study further the effect of the shock on the separated region over the flat-window turret, the temporal variances of the wavefronts on the turret were computed, and the results for different Mach numbers are presented in Fig. 16. Technically, the wake dynamics depends on the position of the flat window, but in reality, the effect is mainly present only at side-looking angles, when the local separation bubble forms over the window. For this reason, wavefronts at side-looking angles were not used to compute the temporal variances and therefore the shock presence is not visible in Fig. 16 for $M = 0.7$ and 0.8. Still, comparing the temporal variances of the wavefronts in Fig. 16 with the ones for the conformal-window turret, presented in Figs. 6 and 7, several conclusions about the shock effect on the wake can be drawn. First, the "quiet valley," although somewhat weaker, is still present for $M = 0.6$. Similar to the conformal-window turret, the quiet valley is reduced at $M = 0.7$ and 0.8. Overall, the temporal variances of the wavefronts in the wake region are very similar between the conformal- and the flat-window turrets, confirming that the presence of the flat window affects the flow primarily at side-looking angles.

Temporal wavefront spectra for different Mach numbers were calculated for a side-looking angle of $\alpha = 90$ deg, presented in Fig. 17, top, and looking through the wake at $\alpha = 120$ deg, shown in Fig. 17, bottom. At the side-looking angle (Fig. 17, top) spectra for $M = 0.5$, 0.6, and 0.7 are similar, with the shear-layer-related peak near $St_D = 1.3$. Only at $M = 0.8$ is the spectrum changed, with the peak moving toward lower frequencies. It further supports the earlier conclusion that the dynamics of the local separation bubble, present over the window at this angle, is not affected by the shock, unless the shock becomes strong enough.

The wake-related normalized wavefront spectra are presented in Fig. 17, bottom. The main peak at $St_D = 1.3$ is unchanged

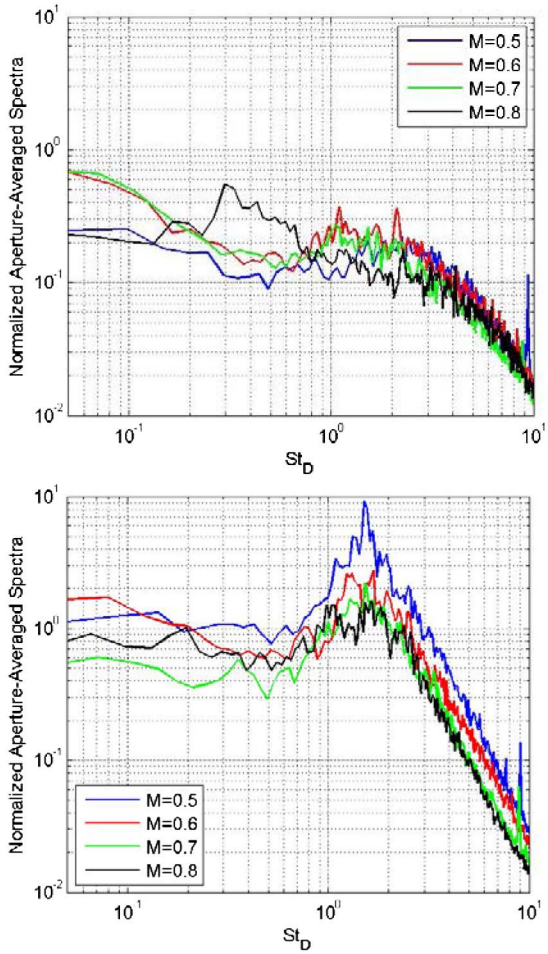

Fig. 17. Aperture-averaged wavefront spectra, $S(f)$, for $\alpha = 90$ deg (top) and for $\alpha = 120$ deg (bottom) at different Mach numbers.

for all tested Mach numbers. The normalized amplitude is the largest for $M = 0.5$ and is approximately the same for higher Mach numbers, providing further evidence that at these speeds the wake is largely unaffected by the shock. Unlike the wavefront spectra at the same viewing angle for the conformal-window turret, shown in Fig. 12, top, wavefronts for the flat-window turret do not appear to exhibit the shack-related modulations at lower frequencies.

5. CONCLUSIONS

Using the AAOL-T program, time-resolved wavefronts were collected in flight for a hemisphere-on-cylinder turret with either conformal or flat windows in a transonic flow regime. Data were taken at different viewing angles, and the aero-optical environment was characterized by computing the overall levels of $\mathrm{OPD_{RMS}}$, as well as the temporal variance of the wavefronts and aperture-averaged wavefront temporal spectra at selected viewing angles. Shock dynamics was studied by using sharp positive gradients in the wavefronts to estimate shock instantaneous locations.

The normalized $\mathrm{OPD_{RMS}}$ was calculated for Mach numbers ranging from 0.5 to 0.8 on both the flat- and conformal-window turrets for different field-of-regard angles. For both geometries, it was found that normalized aero-optical distortions have additional local increase near $\alpha = 80$ deg for the $M = 0.7$ and 0.8. This peak was attributed to the presence of the unsteady shock appearing on top of the turret. The shock location was found to be almost independent of the modified elevation angle; based on optical data, the shock extent appears to increase with increasing Mach number.

The spectra of the shock motion, extracted from optical data, was calculated for $M = 0.7$ and 0.8. For the conformal window the shock-related spectra revealed two peaks at $\mathrm{St}_D = 0.3$ and 0.18 at $M = 0.7$ and only a single peak at $\mathrm{St}_D = 0.15$ at $M = 0.8$. As the $\mathrm{St}_D = 0.15$ was associated in earlier studies with the unsteady motion of the separation line over the turret, it was hypothesized that while at low transonic speeds around $M \sim 0.6$–0.65 the shock has its own dynamics with a higher frequency of $\mathrm{St}_D \sim 0.5$, when the shock grows strong enough to cause a premature separation, it becomes locked with the wake dynamics, having the same frequency as the unsteady separation line. This lock-in mechanism was observed in other studies of the shock–wake interaction.

For the flat-window aperture, only a single peak at $\mathrm{St}_D = 0.15$ was observed at $M = 0.7$ and 0.8 in the shock motion spectra. Based on optical data, the shock dynamics is linked to the local separation bubble over the flat window at side-looking angles, which, in turn, is also linked to the wake dynamics.

The wake-related wavefront spectra in both window geometries revealed a dominant peak at $\mathrm{St}_D = 1.3$, which is associated with small-scale shear-layer structures. The dynamics of the shear-layer structure in the wake was found to be mostly unaffected by the presence of the shock for both window geometries, although some evidence of shock-related modulation at $\mathrm{St}_D = 0.15$ at high Mach number of $M = 0.8$ was noticed for the conformal-window turret. It is expected that this modulation will become stronger at higher transonic Mach numbers.

Future work will include collecting more data using the AAOL-T to acquire more information on the shock motion and to study further the proposed locking mechanism between the shock and wake. Additionally, wind tunnel tests will be performed to gather simultaneous pressure and wavefront measurements to track shock motion and its relation to the separated region motion.

Funding. Joint Technology Office (FA9550-13-1-0001).

Acknowledgment. The U.S. Government is authorized to reproduce and distribute reprints for governmental purposes notwithstanding any copyright notation thereon.

REFERENCES

1. E. J. Jumper, M. Zenk, S. Gordeyev, D. Cavalieri, and M. R. Whiteley, "Airborne aero-optics laboratory," Opt. Eng. **52**, 071408 (2013).
2. C. H. Snyder, M. E. Franke, and M. L. Masquelier, "Wind-tunnel tests of an aircraft turret model," J. Aircraft **37**, 368–376 (2000).
3. R. Sluder, L. Gris, and J. Katz, "Aerodynamics of a generic optical turret," J. Aircraft **45**, 1814–1815 (2008).
4. S. Gordeyev and E. J. Jumper, "Fluid dynamics and aero-optics of turrets," Prog. Aerosp. Sci. **46**, 388–400 (2010).
5. N. De Lucca, S. Gordeyev, E. Jumper, and D. Wittich, "Aero-optical environment around turrets at forward-viewing angles," in *AIAA Aerospace Sciences Meeting, AIAA SciTech Forum* (2013), paper 0721.
6. S. Gordeyev, N. De Lucca, E. J. Jumper, K. Hird, T. J. Juliano, J. W. Gregory, J. Thordahl, and D. J. Wittich, "Comparison of unsteady pressure fields on turrets with different surface features using pressure sensitive paint," Exp. Fluids **55**, 1661 (2014).
7. M. R. Palaviccini, B. George, and L. Cattafesta, "Passive flow control over a three-dimensional turret with a flat aperture," in *AIAA Aerospace Sciences Meeting, AIAA SciTech Forum* (2011), paper 3265.
8. M. Tutkun, P. B. V. Johansson, and B. A. Pettersson Reif, "Visualization and measurement of flow over a cylindrical surface with a bump," AIAA J. **45**, 1763–1770 (2007).
9. H. Zhong, S. Woodig, P. Wang, J. Shang, X. Cui, J. Wang, and T. Liu, "Skin-friction topology of wing-body junction flows," Eur. J. Mech. B **53**, 55–67 (2015).
10. M. M. Tavakol, M. Yaghoubi, and M. M. Motlagh, "Air flow aerodynamic on a wall-mounted hemisphere for various turbulent boundary layers," Exp. Therm. Fluid. Sci. **34**, 538–553 (2010).
11. B. Vukasinovic, A. Glezer, S. Gordeyev, E. Jumper, and W. W. Bower, "Flow control for aero-optics application," Exp. Fluids **54**, 1492 (2013).
12. S. Gordeyev, M. Post, T. MacLaughlin, J. Ceniceros, and E. Jumper, "Aero-optical environment around a conformal-window turret," AIAA J. **45**, 1514–1524 (2007).
13. E. Mathews, K. Wang, M. Wang, and E. Jumper, "LES of an aero-optical turret flow at high reynolds number," in *AIAA Aerospace Sciences Meeting, AIAA SciTech Forum* (2016), paper 1461.
14. E. Mathews, K. Wang, M. Wang, and E. J. Jumper, "LES analysis of hemisphere-on-cylinder turret aero-optics," in *AIAA Aerospace Sciences Meeting, AIAA SciTech Forum* (2014), paper 0323.
15. R. Jelic, S. Sherer, and R. Greendyke, "Simulation of various turret configurations at subsonic and transonic flight conditions using overflow," J. Aircraft **50**, 398–409 (2013).
16. W. J. Coirier, C. Porter, J. Barber, J. Stutts, M. Whiteley, D. Goorskey, and R. Drye, "Aero-optical evaluation of notional turrets in subsonic, transonic and supersonic regimes," in *AIAA Aerospace Sciences Meeting, AIAA SciTech Forum* (2014), paper 2355.
17. C. Porter, J. Seidel, R. Decker, and T. McLaughlin, "Modeling aero-optical distortions around conformal and flat-window turrets for

feedback control," in *AIAA Aerospace Sciences Meeting, AIAA SciTech Forum* (2013), paper 0719.
18. P. E. Morgan and M. R. Visbal, "Effectiveness of flow control for a submerged hemispherical flat-window turret," in *AIAA Aerospace Sciences Meeting, AIAA SciTech Forum* (2013), paper 1015.
19. P. E. Morgan and M. R. Visbal, "Hybrid Reynolds-averaged Navier-Stokes/large-Eddy simulation investigating control of flow over a turret," J. Aircraft **49**, 1700–1717 (2012).
20. J. Ladd, A. Mani, and W. Bower, "Validation of aerodynamic and optical computations for the unsteady flow field about a hemisphere-on-cylinder turret," in *AIAA Aerospace Sciences Meeting, AIAA SciTech Forum* (2009), paper 4118.
21. P. E. Morgan and M. R. Visbal, "Numerical investigation of flow control for a flat-window cylindrical turret," AIAA J. **54**, 861–879 (2016).
22. B. R. Smith, "Application of LES methods to military aircraft flow problems," in *AIAA Aerospace Sciences Meeting, AIAA SciTech Forum* (2010), paper 343.
23. M. Kamel, K. Wang, and M. Wang, "Predictions of aero-optical distortions using LES with wall modeling," in *AIAA Aerospace Sciences Meeting, AIAA SciTech Forum* (2016), paper 1462.
24. C. Porter, S. Gordeyev, M. Zenk, and E. Jumper, "Flight measurements of the aero-optical environment around a flat-windowed turret," AIAA J. **51**, 1394–1403 (2013).
25. N. De Lucca, S. Gordeyev, and E. Jumper, "In-flight aero-optics of turrets," Opt. Eng. **52**, 071405 (2013).
26. E. J. Jumper, "Special section on aero-optics and adaptive optics for aero-optics," Opt. Eng. **52**, 071401 (2013).
27. E. Arad and M. Weidenfeld, "Aero-optic calculations of a spherical turret at transonic flow," in *AIAA Aerospace Sciences Meeting, AIAA SciTech Forum* (2017), paper 0537.
28. C. J. Tam and T. J. Madden, "Investigations of transonic flow over a hemisphere using DES and hybrid RANS/LES turbulence models," in *AIAA Aerospace Sciences Meeting, AIAA SciTech Forum* (2016), paper 1458.
29. J. Morrida, S. Gordeyev, E. Jumper, S. Gogineni, and D. J. Wittich, "Investigation of shock dynamics on a hemisphere using pressure and optical measurements," in *AIAA Aerospace Sciences Meeting, AIAA SciTech Forum* (2016), paper 1348.
30. J. Morrida, S. Gordeyev, and E. Jumper, "Transonic flow dynamics over a hemisphere in flight," in *AIAA Aerospace Sciences Meeting, AIAA SciTech Forum* (2016), paper 1349.
31. S. Gordeyev, A. Vorobiev, E. Jumper, S. Gogineni, and D. J. Wittich, "Studies of flow topology around hemisphere at transonic speeds using time-resolved oil flow visualization," in *AIAA Aerospace Sciences Meeting, AIAA SciTech Forum* (2016), paper 1459.
32. J. Z. Reid, K. P. Lynch, and B. S. Thurow, "Density measurements of a turbulent wake using acetone planar laser-induced fluorescence," AIAA J. **51**, 829–839 (2013).
33. S. J. Beresh, J. F. Henfling, R. W. Spillers, and B. O. M. Pruett, "Unsteady shock motion in a transonic flow over a wall-mounted hemisphere," in *AIAA Aerospace Sciences Meeting, AIAA SciTech Forum* (2013), paper 3201.
34. B. Vukasinovic, A. Glezer, S. Gordeyev, E. Jumper, and V. Kibens, "Active control and optical diagnostics of the flow over a hemispherical turret," in *AIAA Aerospace Sciences Meeting, AIAA SciTech Forum* (2008), paper 0598.
35. S. Fang, K. J. Disotell, S. R. Long, J. W. Gregory, F. C. Semmelmayer, and R. W. Guyton, "Application of fast-responding pressure-sensitive paint to a hemispherical dome in unsteady transonic flow," Exp. Fluids **50**, 1495–1505 (2011).
36. P. E. Morgan, S. E. Sherer, and M. R. Visbal, "Numerical investigation of supersonic flow over a wall-mounted cylinder," in *AIAA Aerospace Sciences Meeting, AIAA SciTech Forum* (2016), paper 0046.
37. A. Vorobiev, S. Gordeyev, E. Jumper, S. Gogineni, A. Marruffo, and D. J. Wittich, "Low-dimensional dynamics and modeling of shock-separation interaction over turrets at transonic speeds," in *AIAA Aerospace Sciences Meeting, AIAA SciTech Forum* (2014), paper 2357.
38. E. J. Jumper, S. Gordeyev, D. Cavalieri, P. Rollins, M. R. Whiteley, and M. J. Krizo, "Airborne aero-optics laboratory—transonic (AAOL-T)," in *AIAA Aerospace Sciences Meeting, AIAA SciTech Forum* (2015), paper 0675.
39. T. S. Ross, "Limitations and applicability of the Maréchal approximation," Appl. Opt. **48**, 1812–1818 (2009).
40. C. Porter, S. Gordeyev, and E. Jumper, "Large-aperture approximation for not-so-large apertures," Opt. Eng. **52**, 071417 (2013).
41. D. J. Goorskey, R. Drye, and M. R. Whiteley, "Dynamic modal analysis of transonic airborne aero-optics laboratory conformal window flight-test aero-optics," Opt. Eng. **52**, 071414 (2013).
42. N. De Lucca, S. Gordeyev, and E. Jumper, "Global unsteady pressure fields over turrets in-flight," in *AIAA Aerospace Sciences Meeting, AIAA SciTech Forum* (2015), paper 0677.